Compressive Beam Alignment for Indoor Millimeter-Wave Systems

April Junio, Rafaela Lomboy*, Raj Sai Sohel Bandari, and Mohammed E. Eltayeb
Department of Electrical & Electronic Engineering
**Department of Computer Science*
California State University, Sacramento, Sacramento, USA
Email: {apriljunio, rlomboy, rbandari, mohammed.eltayeb}@csus.edu

2025 IEEE 22nd Consumer Communications & Networking Conference (CCNC) | 979-8-3315-0805-0/25/$31.00 ©2025 IEEE | DOI: 10.1109/CCNC54725.2025.10976196

***Abstract*—Traditional compressed sensing (CS) based beam alignment techniques enable swift mm-wave connectivity with a limited number of measurements. These techniques, however, rely on prior knowledge of the communication channel model and the user's array manifold to design the sensing matrix and minimize angle quantization errors. This limits their effectiveness in dynamic environments. Unlike prior work that rely on knowledge of the user's antenna architecture, beamforming codebook, and channel, this paper introduces a CS-based beam alignment technique that is agnostic to these factors. The proposed formulation eliminates angle quantization errors by mapping the recovered angular directions directly onto the user's specific beamforming codebook. Experimental results at 60 GHz demonstrate successful recovery of the mm-wave power distribution in the angular domain. This facilitates accurate beam alignment with limited measurements when compared to exhaustive search solutions.**

***Index Terms*—Millimeter-wave communications, indoor beam alignment, discrete cosine transform, compressed sensing.**

I. Introduction

The demand for low latency and high-speed communications to support next generation technology and applications is on the rise [1]. The abundance of bandwidth in the millimeter-wave (mm-wave) band enables service providers to meet those demands [2]. However promising, the deployment of mm-wave communication systems is challenged by the sensitivity to line-of-sight (LoS) link blockages and requires precise alignment of the communication beams. While existing techniques such as codebook-based hierarchical beam training and compressed channel estimation have been proposed to address these challenges [3]–[6], they exhibit limitations in dense indoor environments where intermittent blockages are imminent. Furthermore, these techniques require knowledge of the complete array response of all receivers, do not account for potential distortions introduced by the antenna front-end hardware, and often rely on a pre-defined channel model, which might not accurately reflect real-world conditions. To address these limitations, novel methods that ensure robust performance in dynamic indoor environments, regardless of the transceiver's antenna configuration, are required.

Compressed sensing (CS) has emerged as a promising signal processing technique for swift mm-wave channel estimation due to its ability to exploit channel sparsity. Nonetheless, existing CS-based mm-wave beam alignment techniques primarily focus on outdoor environments [6], [7]. Outdoor environments are generally static, and mm-wave propagation channels exhibit spatial sparsity [7]. This sparsity aligns well with the assumptions of compressed sensing. Conversely, indoor environments present a unique challenge due to the presence of numerous objects that significantly affect signal propagation, resulting in increased scattering and potentially less sparse channels. Fig. 1 illustrates this by plotting the received signal strength (RSS) measurements obtained at a line-of-sight (LoS) receiver within an indoor lab environment. The figure shows that the strongest signal is received directly between the transmitter and receiver (LoS). However, there are also significant signal reflections and scattering from objects in the environment, leading to additional signal peaks at non-LoS (NLoS) angles. This scattering profile underscores the key difference between indoor and outdoor mm-wave channels.

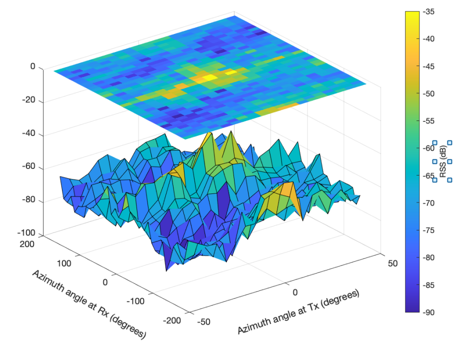

Fig. 1. RSS measurements versus beam orientation for a 16-element phased antenna array operating at 60 GHz in a 58^2 m indoor lab environment.

This paper presents a novel CS approach for beam alignment in indoor mm-wave environments. We depart from prior CS-based methods which rely on prior knowledge of the communication channel model and array manifold. Instead, we introduce a framework that leverages the discrete cosine transform (DCT) to achieve sparsity and approximate the directions of the strongest channel clusters (power) in the transform domain. This framework offers two key advantages: (i) model-agnostic operation as it eliminates the need for prior knowledge of the channel model, and ii) device-specific operation by directly mapping angles-of-arrival (AoA) and/or

979-8-3315-0805-0/25/$31.00 ©2025 IEEE

angles-of-departure (AoD) to the user's quantized codebook. This is achieved by sampling power measurements at random directions and exploiting the energy compaction property of the DCT to recover a compressed representation that closely approximates the original spatial domain power distribution. This behavior is analogous to a low-pass filter in image processing, which blurs the image but can reconstruct missing information to some extent. To the best knowledge of the authors, this work represents the first implementation of CS-based beam alignment in a realistic indoor dense environment.

II. System Model and Problem Formulation

A. System Model

We consider a system where a stationary mm-wave access point (AP) with t antennas communicates with a stationary single receiver equipped with r antennas. The access point uses one of p beamforming vectors present in its codebook $\boldsymbol{\mathcal{F}} = \{\mathbf{f}_1, \mathbf{f}_2, ..., \mathbf{f}_p\}$, and similarly, the receiver uses one of its q combining vectors in its codebook $\boldsymbol{\mathcal{W}} = \{\mathbf{w}_1, \mathbf{w}_2, ..., \mathbf{w}_q\}$ for communication. The beamforming vector $\mathbf{f}_i \in \mathcal{C}^{t\times 1}$ steers the transmit beam towards the angle θ_i, and similarly, the combining vector $\mathbf{w}_j \in \mathcal{C}^{r\times 1}$ at the receiver steers the receiver's beam towards the angle θ_j. Let s, $\mathbb{E}[|s|^2] = 1$, be the complex symbol transmitted by the AP to the receiver using the beamformer $\mathbf{f}_j$, the received signal at the receiver using the combing vector $\mathbf{w}_i$ is given by $y = \mathbf{w}_i^* \mathbf{H} \mathbf{f}_j s + e$, where $i = 1, 2, .., q$, $j = 1, 2, ..., p$, and $\mathbf{e} \sim \mathcal{CN}(0, \sigma_e^2)$ represents the additive white Gaussian noise with a complex normal distribution. The matrix $\mathbf{H}$ of size $r \times t$ represents the unknown mm-wave channel between the AP and the receiver.

B. Problem Formulation

In this paper, the received power at the receiver is adopted as the performance metric. Therefore, optimal transmit and receive beam selection occurs when the AP and the receiver pick the beamforming and combining vectors that maximizes the received power at the receiver, i.e. $\mathbb{E}[|y|^2]$. This is achieved by selecting the ideal transmit beamforming vector $\mathbf{f}^\star$ and receive combining vector $\mathbf{w}^\star$ as follows

$$< \mathbf{f}^\star, \mathbf{w}^\star > = \arg \max_{\mathbf{w}\in\boldsymbol{\mathcal{W}}, \mathbf{f}\in\boldsymbol{\mathcal{F}}} |\mathbf{w}^* \mathbf{H} \mathbf{f}|^2. \tag{1}$$

Without explicit knowledge of the channel $\mathbf{H}$, the optimal transmit and receive vectors can be obtained via an exhaustive search encompassing all codebook entries. However, this approach suffers from high computational complexity, making it impractical for real-world scenarios. In the next section, we propose a method that identifies the angular distribution of the strongest channel clusters without the need for an exhaustive search process.

III. Proposed MM-Wave Beam Alignment Solution

A. Initial Beam Measurements

To initiate sensing, the transmitter transmits m_1 beams using randomly selected m_1 beamforming vectors from its codebook $\boldsymbol{\mathcal{F}}$. Similarly, the receiver uses randomly selects m_2 combining vectors from its codebook $\boldsymbol{\mathcal{W}}$ for each transmit beam to capture projections of the spatial distribution of the signal strength as follows

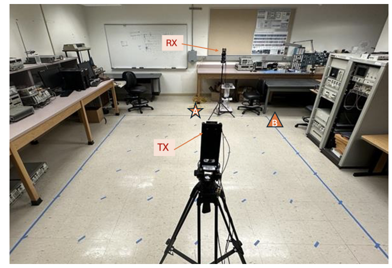

Fig. 2. View of the mm-wave propagation environment. The transmit and receive antennas were situated 4.3 meters (Location A) and 4.5 meters (Location B) apart. Antennas heights are set to 1.6 meters.

$$\mathbf{Y} = |\mathbf{W}_{m_2}^* \mathbf{H} \mathbf{F}_{m_1} + \mathbf{E}|^2. \tag{2}$$

The matrix $\mathbf{Y} \in \mathbb{C}^{m_2\times m_1}$ contains the sampled signal strength measurements using $m = m_1 m_2$ transmit and receive beams, the combing matrix $\mathbf{W}_{m_2} \in \mathbb{C}^{r\times m_2}$ consists of m_2 combining vectors randomly selected from the codebook $\boldsymbol{\mathcal{W}}$, the beamforming matrix $\mathbf{F}_{m_1} \in \mathbb{C}^{t\times m_1}$ consists of m_1 beamforming vectors randomly selected from the codebook $\boldsymbol{\mathcal{F}}$, and $\mathbf{E} \in \mathbb{C}^{m_2\times m_1}$ is the complex additive noise matrix.

B. Sparse formulation for recovering missing measurements

For ease of exposition, we omit the effect of noise and rewrite (2) as

$$\begin{aligned} \tilde{\mathbf{Y}} &= |\mathbf{W}_{m_2}^* \mathbf{H} \mathbf{F}_{m_1}|^2 = |\mathbf{S}_2 \mathbf{W}_q^* \mathbf{H} \mathbf{F}_p \mathbf{S}_1|^2 & (3) \\ &= \mathbf{S}_2 |\mathbf{W}_p^* \mathbf{H} \mathbf{F}_q|^2 \mathbf{S}_1 = \mathbf{S}_2 \boldsymbol{\Phi} \mathbf{S}_1. & (4) \end{aligned}$$

In (3), we expressed $\mathbf{W}_{m_2}^*$ as $\mathbf{S}_2 \mathbf{W}_q^*$ and $\mathbf{F}_{m_1}$ as $\mathbf{F}_p \mathbf{S}_1$. The combining matrix $\mathbf{W}_q$ consists of of all the combining vectors in $\boldsymbol{\mathcal{W}}$, and the beamforming matrix $\mathbf{F}_p$ consists of all the vectors in $\boldsymbol{\mathcal{F}}$. The random selection matrices $\mathbf{S}_1 \in \mathbb{R}^{p\times m_1}$ and $\mathbf{S}_2 \in \mathbb{R}^{m_2\times q}$ are binary matrices where each row has a cardinality (number of "1"s) of 1, and each column has a cardinality of at most 1. The unknown matrix $\boldsymbol{\Phi} = |\mathbf{W}_p^* \mathbf{H} \mathbf{F}_q|^2$ is of size $p \times q$ and carries the projections of mm-wave signal strength across all transmit and receive codebooks entries. This matrix is unknown and can be estimated via exhaustive search over all transmit and receive beams. This brute force approach necessitates a total of $n = pq$ measurements, where p and q represent the dimensions of the transmit and receive codebooks, respectively.

Vectorizing the matrix $\tilde{\mathbf{Y}}$ in (4) yields

$$\tilde{\mathbf{y}} = \underbrace{\mathbf{S}_2^T \otimes \mathbf{S}_1}_{\mathbf{A}} \underbrace{\text{Vec}(\boldsymbol{\Phi})}_{\mathbf{x}}, \tag{5}$$

where $\tilde{\mathbf{y}} = \text{Vec}(\tilde{\mathbf{Y}})$ and $\otimes$ is the Kronecker product operator. While the matrix $\boldsymbol{\Phi}$ might not be inherently sparse in the spatial domain, we exploit the energy compaction property of the DCT to enforce $\boldsymbol{\Phi}$ be sparse in the DCT domain. The DCT has the property of concentrating the signal's energy

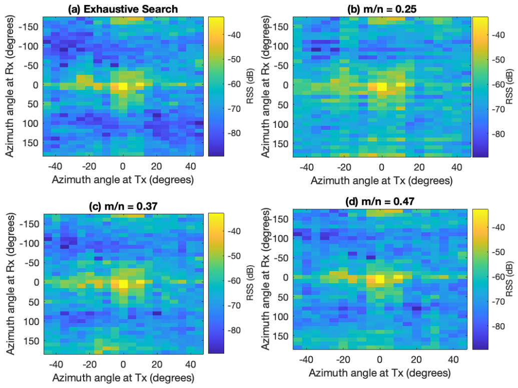

Fig. 3. RSS versus the TX/RX beam orientation at location A when using (i) exhaustive search over all TX/RX angles (top left figure), (ii) CS recovery with $(m/n = 0.25)$, (iii) CS recovery with $(m/n = 0.37)$, and (iv) CS recovery with $(m/n = 0.47)$.

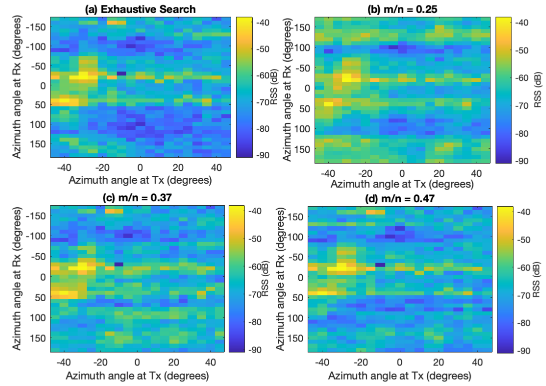

Fig. 4. RSS versus the TX/RX beam orientation at location B when using (i) exhaustive search over all TX/RX angles (top left figure), (ii) CS recovery with $(m/n = 0.25)$, (iii) CS recovery with $(m/n = 0.37)$, and (iv) CS recovery with $(m/n = 0.47)$.

into a few coefficients, particularly the low-frequency ones. By neglecting the higher-frequency DCT coefficients of $\mathbf{\Phi}$, we enforce sparsity in the transformed domain. Using compressed sensing, an approximation to the DCT of $\mathbf{\Phi}$ is obtained and used to compute an approximation of $\mathbf{\Phi}$ in the spatial domain.

C. Compressed sensing recovery

To recover $\mathbf{x}$ in the transform domain rewrite (5) as follows

$$\tilde{\mathbf{y}} = \mathbf{A}\mathbf{x} = \mathbf{A}\mathbf{\Psi}^{-1}\hat{\mathbf{x}}. \tag{6}$$

In (6), $\mathbf{\Psi}^{-1}$ represent the inverse DCT matrix, and $\hat{\mathbf{x}}$ carries the DCT coefficients of the power measurement vector $\mathbf{x} = \text{Vec}(\mathbf{\Phi})$. The vector $\hat{\mathbf{x}}$, can be recovered by solving the following ℓ_0-minimization problem

$$\min \|\hat{\mathbf{x}}\|_0 \quad \text{s.t. } \tilde{\mathbf{y}}= \mathbf{A}\mathbf{\Psi}^{-1}\hat{\mathbf{x}}. \tag{7}$$

To leverage the scattering conditions of the environment, where higher scattering corresponds to more higher frequency coefficients, we adopt the weighted LASSO to recover $\hat{\mathbf{x}}$. The weighted LASSO estimate of (7) is given by [8] as $\arg\min_{\hat{\mathbf{x}}\in\mathbb{R}^{n\times 1}} \|\mathbf{y} - \mathbf{A}\mathbf{\Psi}^{-1}\hat{\mathbf{x}}\|_2^2 + \tau\|\hat{\mathbf{x}}\|_{\boldsymbol{\omega},1}$, where $\|\hat{\mathbf{x}}\|_{\omega,1} = \sum_{i=1}^{n}\omega_i|\hat{x}_i|$, the weights $\omega_i = -\log p_i$, p_i being the probability the $i-th$ entry of $\hat{\mathbf{x}}$ is non-zero and can be adjusted based on the scattering environment, and τ is a regularization parameter. The recovered vector $\hat{\mathbf{x}}$ is rearranged to obtain $\hat{\mathbf{\Phi}}$.

D. Optimal beam selection

The indices of optimal beamforming/combining vector pair $(i^\star, j^\star)$ that correspond to the maximum estimated received signal strength is selected as follows $< i^\star, j^\star >= \arg\max_{i,j} \hat{\mathbf{\Phi}}_{i,j}$, where $i = 1, ..., p$, and $j = 1, ..., q$. The selected transmit beamforming vector is $\mathbf{f}^\star = \boldsymbol{\mathcal{F}}_{:,i^\star}$ and the selected receive combining vector is $\mathbf{w}^\star = \boldsymbol{\mathcal{W}}_{:,j^\star}$

IV. Measurement Setup and Methodology

Indoor measurements were conducted in a lab environment with surfaces of varying materials including wood panel, glossy white-board, metal cabinets, and other environmental clutter as shown in Fig. 2. The transmitter (TX) was positioned at a fixed location, while the receiver (RX) was positioned at two locations, namely location A and B. At Location A, the receiver is aligned with the transmitter to create a LoS link. At Location B, the receiver is situated adjacent to a metallic equipment rack thereby resulting in an additional anticipated cluster as shown in Fig. 4.

A. Phased antenna array setup

Two 60 GHz mm-wave phased antenna array transceiver kits (Sivers EVK02001) [9] were used for measurements as depicted in Fig. 2. The beam direction can be electronically steered from +45 to -45 degrees in the azimuth plane. Each antenna kit includes a 16 element antenna patch antenna module that is steered using codebooks $\boldsymbol{\mathcal{F}}, \boldsymbol{\mathcal{W}}$. The transmit and receive codebooks can be found in [10].

B. Measurement procedure

A universal software radio peripheral (USRP) is used to generate a sinusoidal signal with a sampling rate of 1 MHz. The phased antenna array kit up converts this signal to 60 GHz before transmission to the receiver. The receiver kit and USRP downconvert the received signal back to baseband. The power spectrum of the down converted signal is computed using a flattop window filter. To capture signal strength measurements across various angles, the receiver is steered in the azimuth plane in the range -180^o, to 180^o in increments of 10^o. Similarly, the transmit angles are electronically steered from +45 to -45 degrees in increments of 5 degrees in the azimuth plan. The received signal strength is extracted from the FFT power spectrum for each receive angle.

V. Experimental Results and Discussions

In this section, we use real-world data to test the performance of the proposed compressed beam alignment technique outlined in Sec. III using the measurement setup outlined in Sec. IV. We analyze the efficacy of the proposed

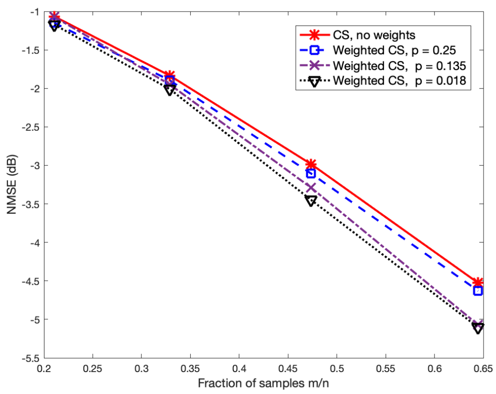

Fig. 5. NMSE of the recovered RSS versus the fraction of CS measurements at location A. To prioritize the lower frequency components, the first 75% of $\hat{\mathbf{x}}$, are assigned a weight of 1, while the remaining 25% are assigned a weight $w = -\log p$.

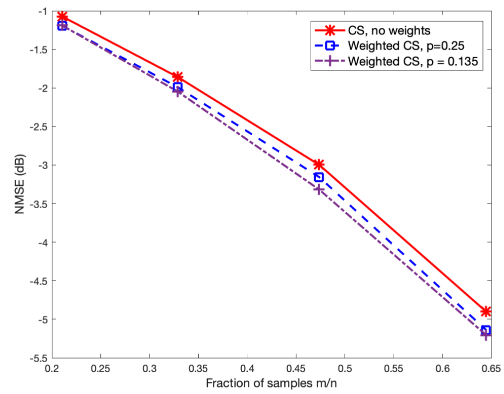

Fig. 6. NMSE of the recovered RSS versus the fraction of CS measurements at location B. The first 75% of $\hat{\mathbf{x}}$, are assigned a weight of 1, while the remaining 25% are assigned a weight $w = -\log p$.

beam alignment technique based on measured RSS. The transmit codebook $\mathcal{F}$ consists of 19 beam steering vectors, while the receive codebook $\mathcal{W}$ consists of 36 entries.

In Fig. 3 random samples were taken at Location A and the proposed CS technique is applied to recover the power distribution across the complete angular domain. When the number of measurements/samples are 171, corresponding to a ratio of $m/n = \frac{171}{684} = 0.25$, the proposed technique was able to identify the location of the strong cluster, however, we see also observe some false positives, i.e. power at random angles, when compared to the exhaustive search method. We also observe that these false positives diminish with higher number of measurements. This trend is observed at Location B as shown in Fig. 4.

Fig. 5 and Fig. 6 illustrate the normalized mean square error (NMSE) at Locations A and B calculated as $\frac{\|\mathbf{\Phi}-\hat{\mathbf{\Phi}}\|_2^2}{\|\mathbf{\Phi}\|_2^2}$, to calculate the average RSS reconstruction error. Both figures show a decrease in NMSE as the number of measurements increases when no weights are applied. By applying weights to the last 25% of the vector $\hat{\mathbf{x}}$, we observe an improvement in NMSE with lower probability, p, in both figures. This suggests that exploiting the sparsity pattern in $\hat{\mathbf{x}}$ can enhance detection performance. The improvement gap for Location B (with and without weights), however, is smaller than that of Location A due to higher scattering at Location B which leads to a less sparse representation. To further optimize performance, future work will focus on adaptive weight selection strategies that can make use of prior environment information and adjust to the scattering characteristics of the communication environment.

VI. Conclusions

In this paper, we proposed and experimentally evaluated a novel mm-wave beam alignment technique specifically suited for dense indoor environments. Experimental results demonstrate that the proposed technique significantly reduces the beam alignment overhead compared to exhaustive search methods, thus making it highly attractive for practical mm-wave deployments in dense indoor environments. Future work will focus on beam alignment for multi-user scenarios and leveraging environment scattering information to further reduce the fraction of samples required for beam alignment by optimizing the weight selection strategy.

Acknowledgment

This material is based on work supported by the National Science Foundation under grant No. NSF-2243089.

References

[1] J. Zhang et al., "A Survey of mmWave-Based Human Sensing: Technology, Platforms and Applications," in *IEEE Commun. Surv. Tutor.,* vol. 25, no. 4, pp. 2052-2087, Fourthquarter 2023.

[2] T. S. Rappaport, Y. Xing, O. Kanhere, S. Ju, A. Madanayake, S. Mandal, A. Alkhateeb, and G. C. Trichopoulos, "Wireless communications and applications above 100 GHz: Opportunities and challenges for 6G and beyond," IEEE Access, vol. 7, pp. 78 729–78 757, 2019.

[3] S. Hur, T. Kim, D. J. Love, J. V. Krogmeier, T. A. Thomas, and A. Ghosh, "Millimeter wave beamforming for wireless backhaul and access in small cell networks,," *IEEE Trans. Commun.,* vol. 61, no. 10, pp. 4391–4403, 2013.

[4] M. E. Eltayeb, A. Alkhateeb, R. W. Heath, and T. Y. Al-Naffouri, "Opportunistic beam training with hybrid analog/digital codebooks for mmwave systems," in *IEEE GlobalSIP,* 2015, pp. 315–319.

[5] M. E. Eltayeb, T. Y. Al-Naffouri and H. R. Bahrami, "Compressive Sensing for Feedback Reduction in MIMO Broadcast Channels," in *IEEE Trans. Commun.,* vol. 62, no. 9, pp. 3209-3222, Sept. 2014.

[6] A. Alkhateeb, O. El Ayach, G. Leus and R. W. Heath, "Channel Estimation and Hybrid Precoding for Millimeter Wave Cellular systems," in *IEEE J. Sel. Topics Signal Process,* vol. 8, pp. 831-846, Oct. 2014.

[7] E. Khordad, I. B. Collings, S. V. Hanly and G. Caire, "Compressive Sensing-Based Beam Alignment Schemes for Time-Varying Millimeter-Wave Channels," *IEEE Trans. Wireless Commun.*, vol. 22, no. 3, pp. 1604-1617, March 2023.

[8] J. Scarlett, J. S. Evans and S. Dey, "Compressed Sensing With Prior Information: Information-Theoretic Limits and Practical Decoders," in *IEEE Trans. Signal Process.* , vol. 61, no. 2, pp. 427-439, Jan.15, 2013,

[9] SiversIMA, "Product brief: EVK06002, " 2021. [Online]. Available: https://www.sivers-semiconductors.com/wp-content/uploads/2021/10/Product-Brief-EVK06002-202110.pdf.

[10] A. Alkhateeb, G. Charan, T. Osman, A. Hredzak, N. Srinivas, U. Demirhan, and J. Morais, "DeepSense 6G: A Large-Scale Real-World Multi-Modal Sensing and Communication Dataset," *IEEE Dataport*, October 31, 2022.